An Optical Array Receiver for Deep-Space Communication through Atmospheric Turbulence

V. Vilnrotter,[1] C.-W. Lau,[1] M. Srinivasan,[1] R. Mukai,[1] and K. Andrews[1]

The theoretical foundations of an optical array receiver consisting of relatively small telescopes are developed and analyzed. It is shown that optical array receivers can be designed to perform as well as a large single-aperture receiver on the ground, while enjoying significant advantages in terms of operational reliability, ease of future expansion to achieve greater capacity, and further advantages in terms of cost and implementation due to the highly parallel architecture inherent in the array design. Optical array receivers for deep-space communication applications are analyzed using the accepted modal analysis for background radiation; however, the signal fields are represented using a novel aperture-plane expansion that takes into account the characteristics of atmospheric turbulence. It is shown, based on this analysis, that for ground-based reception the number of array elements can be increased without suffering any performance degradation, as long as the telescope diameters exceed the coherence length of the atmosphere. Maximum-likelihood detection of turbulence-degraded signal fields using an array of telescopes, each equipped with its own focal-plane detector array to mitigate turbulence effects, is developed for the case of pulse-position modulated signals observed in the presence of background radiation. The performance of optical array receivers then is compared to single-aperture receivers with diameters ranging from 4 to 8 meters, both in the presence of turbulence relevant to ground-based reception and in a hypothetical turbulence-free environment; it is shown that without atmospheric turbulence to break up the signal fields prior to detection, as would be the case in space, single-aperture receivers outperform receiver arrays whenever significant background radiation is present. However, for ground-based reception of deep-space signals, we demonstrate that the number of array elements can be as great as several thousand without incurring any performance degradation relative to a large single-aperture optical receiver.

---

[1] Communications Systems and Research Section.

The research described in this publication was carried out by the Jet Propulsion Laboratory, California Institute of Technology, under a contract with the National Aeronautics and Space Administration.

I. Introduction

Earth-based reception of deep-space optical signals using an array of relatively small telescopes together with high-speed digital signal processing is a viable alternative to large-aperture telescopes for receiving deep-space optical signals. Large-aperture telescopes are costly to build and operate, and inherently suffer from single-point failure in case of malfunction, thus jeopardizing precious data. Performance of a properly designed array tends to degrade gracefully in case of element failures, even without replacement, but the array approach also provides the option to switch in spare telescopes in case of failure, without a significant increase in cost. However, the equivalence of the array receiver and the single large telescope under operating conditions of interest remains to be demonstrated; establishing that theoretical equivalence and clarifying the similarities and differences between the two approaches is the goal of this article.

The premise of a single-aperture optical receiver for deep-space telemetry is to employ one large (approximately 10-meter) primary reflector, possibly segmented, with custom optics designed to focus the turbulence-degraded optical fields onto a large-area detector. Due to the large mirror size, diffraction-limited performance is difficult to attain at reasonable cost, and in addition the large optics require a massive and costly mechanical support and tracking system. If, instead, we consider building an optical receiver array using relatively small but high-quality off-the-shelf telescopes, we will be able to meet requirements in a cost-effective manner with the added benefit that development, testing, and evaluation costs can be greatly reduced. This follows because with an array all the elements are identical, and the fundamental interconnectivity and arraying concepts can be demonstrated with just a few elements; for example, a small array consisting of two or three telescopes can be used to demonstrate virtually all of the necessary arraying concepts relatively cheaply, and the results can be extrapolated with confidence to a much larger array. Not so with a receiver relying on a single huge reflector; a single large-aperture telescope has additional unique features and problems that a small telescope prototype will not reveal. The difficulty of constructing and aligning a large optical telescope, segmented aperture or otherwise, is in itself a daunting task, exacerbated by the additional problems that gravitational loading produces on the backup structure and drive mechanism.

In addition to a favorable cost and risk trade-off, the optical array receiver approach has advantages in terms of implementation complexity and performance for several key communications functions that need to be clarified and evaluated. These characteristics can best be explained in terms of an array receiver model that emphasizes the communications aspects of the optical array. We begin by developing the underlying concepts governing the behavior of optical arrays. Next, similarities and differences between single-aperture and array telescopes designed for reception of deep-space telemetry will be explored, followed by a detailed investigation of communications performance. We conclude with a comparison of array receivers with the more conventional large-aperture optical receiver under realistic operating conditions.

II. The Optical Array Receiver Concept

The essential difference between a single-aperture optical communications receiver and an optical array receiver is that a single aperture focuses all of the light energy it collects onto the surface of an optical detector before detection, whereas an array receiver focuses portions of the total collected energy onto separate detectors, optically detects each fractional energy component, and then combines the electrical signal from the array of detector outputs to form the observable, or "decision statistic" used to decode the telemetry signal. Thus, an optical interferometer that attempts to synthesize a huge aperture with a few sparsely spaced elements to increase resolution really counts as a single-aperture receiver according to this definition, even though it appears to be composed of disconnected elements much like an array. The point is that with an interferometer the light from the interferometer elements is combined coherently before detection, whereas in a communications array, according to our definition, light is detected at each element first, followed by post-detection processing to construct the desired signal. A single-aperture receiver need not be constructed from a single monolithic glass lens or reflector

element; large modern telescopes generally are constructed from hexagonal segments with each surface placed near its neighbors and monitored to form a single parabolic surface. Alternatively, this type of construction can be thought of as a "dense interferometer," where the high-resolution partial image due to the distant outer elements is filled in completely to reconstruct the image in real time (instead of the conventional "sparse interferometer," where post-processing typically is required to reconstruct the image after the observation). If the image of a point source were formed using every segment of the surface and then detected, that collection of segments would be considered a single-aperture receiver. However, if the focal spot of each segment were separated from the rest and detected with a separate detector element or focal-plane detector array, that would constitute an array receiver in the framework of our definition. Note that a focal-plane array in a single telescope might be construed as an optical array receiver under this definition, but the intent is for there to be multiple apertures. This construction serves as a convenient conceptual vehicle to illustrate the similarities and differences between single-aperture and multi-aperture array receivers.

A conceptual block diagram of an optical array receiver suitable for deep-space telemetry reception is shown in Fig. 1, intended to identify the key components required for array receiver operation. The most conspicuous feature of an optical array receiver is a large number of small- to medium-sized telescopes, with the individual apertures and number of telescopes designed to make up the desired total collecting area. This array of telescopes is envisioned to be fully computer controlled via the user interface, and predict-driven to achieve rough pointing and tracking of the desired spacecraft. Fine-pointing and tracking functions then take over to keep each telescope pointed towards the source despite imperfect pointing predicts, telescope drive errors, and vibration caused by light wind.

The optical signal collected by each telescope is focused onto a detector array located in the focal plane, designated as the focal-plane array, or FPA. Despite atmospheric turbulence degrading the coherence of the received signal fields and interfering background radiation entering the receiver along with the signal within the passband of the optical pre-detection filter, the FPA and associated digital signal-processing electronics extract real-time pointing information, keeping the centroid of the turbulent time-varying

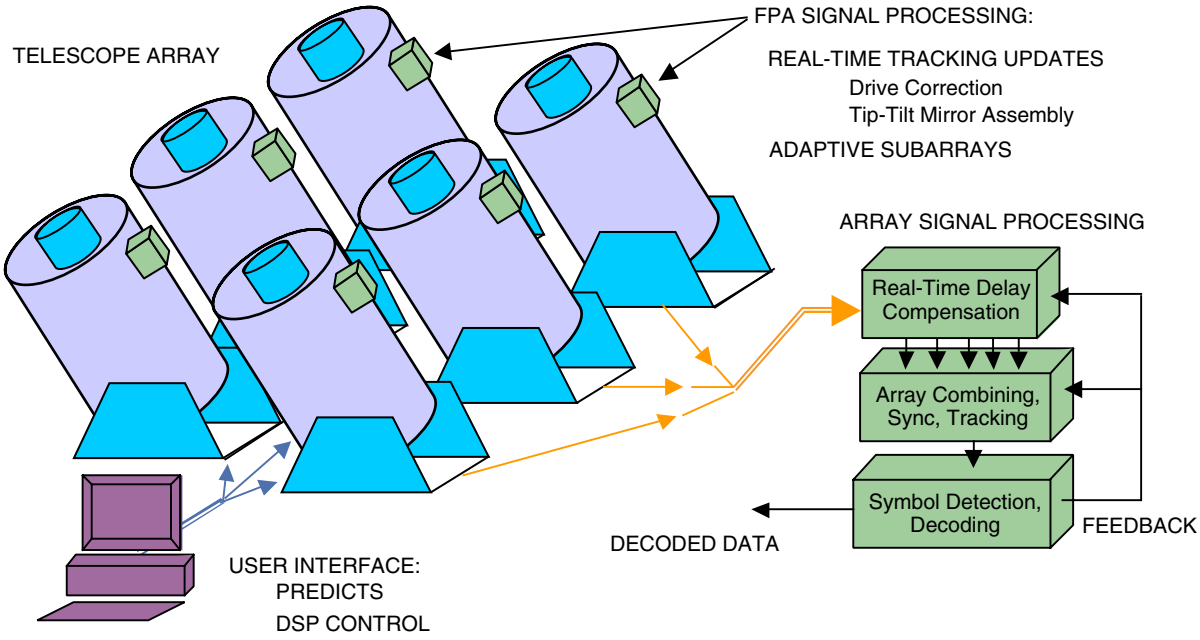

Fig. 1. Conceptual design of an optical array receiver, illustrating key functions required for array reception: the telescope array; focal-plane pre-processing of the signal at each telescope; and the additional array processing needed to combine the pre-processed signals and decode the received data.

signal centered over the FPA. This is accomplished in two steps: first, large accumulated pointing errors are fed back to the telescope drive assembly, repointing the entire instrument; and second, small excursions of the signal distribution from the center of the array are corrected via a fast-response tip–tilt mirror that responds to real-time pointing updates generated by the FPA electronics. In addition, the short-term average signal energy over each detector element is measured and used to implement various adaptive background-suppression algorithms to improve or optimize the communications performance of the entire array.

The electrical signals generated at each telescope by the FPA signal-processing assembly are collected at a central array signal-processing station, where the final operations necessary for data decoding are carried out. The relative time delay between signals from various telescopes is measured and removed, effectively aligning each signal stream in time before further processing is carried out. The delay-compensated signals then are combined in a manner to optimize array performance, and further processed to affect symbol synchronization, frame synchronization, Doppler compensation, and to effectively maintain lock between the combined signal and the receiver time frame. At this point, the transmitted channel symbols are detected, and the decoding operation begins. The detected channel symbols now could be handed over to a hard-decision decoder or various forms of soft-decision decoding could be implemented through the use of additional side information along with the detected symbols. The channel symbols detected by the array receiver also may be used to aid the delay compensation, array combining, and synchronization operations.

III. Aperture-Plane Expansions

It is common practice in the optical communications literature to expand random fields at the telescope aperture into spatial modes that are closely related to diffraction-limited fields of view, clustered to form a complete orthonormal set of functions that essentially samples the field of view (FOV) of the receiver. This concept is illustrated in Fig. 2, where a cluster of diffraction-limited fields of view (denoted Ω_{dl}) is shown collecting light energy from both signal and background radiation with slightly different angles of arrival. If it can be shown that each element of the set of spatial modes satisfies an integral equation whose kernel is the field coherence function over the aperture, then each sample function of the field can be expanded into an orthonormal series with uncorrelated coefficients, also known as a Karhounen–Loeve expansion [1].

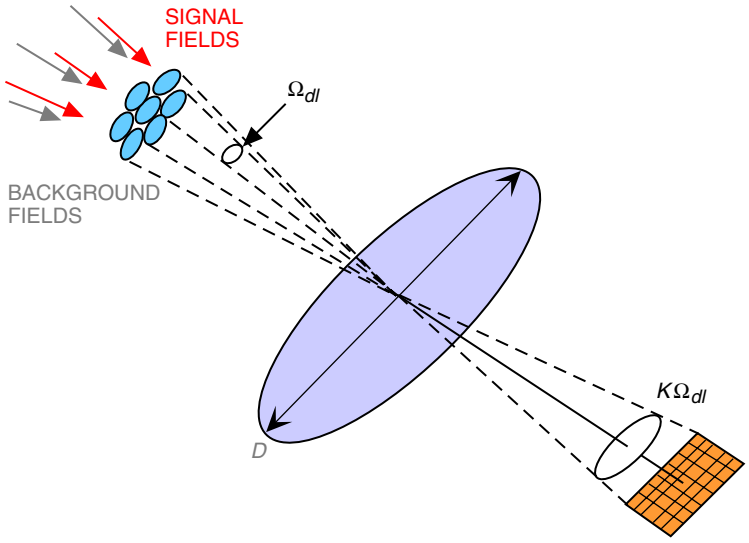

Fig. 2. Plane-wave expansion of aperture-plane fields: diffraction-limited FOV interpretation.

When applying this model to the array receiver, it is more appropriate to view the received turbulence-degraded optical fields as "frozen" over time scales of milliseconds, the characteristic time scale of turbulence, during which time a great many optical data symbols are received. It is advantageous to view each sample function of the received field as a frozen realization of a two-dimensional field, representing a certain epoch in time over which the stationary model applies, as a deterministic two-dimensional function defined over the aperture plane of the receiver. This enables the application of well-known sampling theory to the fields, resulting in a model that clarifies the array receiver concept and contributes to the development of a useful engineering model.

Plane-wave expansions are especially useful for characterizing the effects of background radiation. In Fig. 2, both signal and background power are shown entering the receiver through each diffraction-limited FOV. If the diameter of the receiver is smaller than the coherence length of the signal field (a condition that can be met in the vacuum of space or even on the ground with very small apertures), then all of the signal energy is concentrated into a diffraction-limited point-spread function (PSF) in the focal plane. In effect, the signal appears to originate from a point source an infinite distance from the receiver. For the case of receiving spatially coherent signal fields, the signal power collected by a diffraction-limited telescope under ideal conditions is therefore proportional to the collecting area. The model for background radiation is somewhat more complicated, since background radiation is an extended source with respect to the narrow FOV of typical optical receivers. Surprisingly, the background power collected by a diffraction-limited telescope does not depend on the collecting area, but instead is a constant that depends only on the brightness of the source and the bandwidth of the optical filter at the wavelength of interest, λ. This can be shown by examining the units of the spectral radiance function, $N(\lambda)$, used to quantify background radiation: the units of the spectral radiance functions are power (microwatts) per receiver area (square meters), field of view (steradians), and optical filter bandwidth (angstroms or nanometers). The background power collected by a diffraction-limited receiver is given by [3]

$$P_b = N(\lambda)\Delta\lambda\Omega_{dl}A_r$$

where $\Delta\lambda$ is the optical filter bandwidth and A_r is the collecting area. Since the diffraction-limited field of view is inversely related to area, i.e., $\Omega_{dl} \approx \lambda^2/A_r$, we have

$$P_b^* \approx N(\lambda)\Delta\lambda\lambda^2$$

and therefore the background power collected by a diffraction-limited receiver, P_b^*, is independent of receiver area. Therefore, all diffraction-limited receivers of whatever size collect the same background power when observing a given background distribution, independent of receiver collecting area.

The distorted optical fields resulting from atmospheric turbulence are necessarily bandlimited, since the "image" of a point source observed through turbulence is of finite extent. This conclusion is based on the observation that any complex field distribution over the aperture plane is the Fourier transform of the complex "image" function generated in the focal plane [4,5], which therefore represents the wave-number space of the aperture. In order to determine the extent of significant wave numbers of representative optical field distributions, sample functions generated from Kolmogorov phase screens were analyzed. Representative examples of the resulting aperture-plane coherence function and its Fourier transform, representing the two-dimensional power spectrum of the field in wave -number space, are shown in Figs. 3 and 4, for the case of 10-cm atmospheric coherence length, or $r_0 = 0.1$ meter.

If we can show that the received fields over the aperture are wavenumber-limited two-dimensional functions, then we can invoke a two-dimensional version of the sampling theorem, as described in [5]. This enables the expansion of the received fields using two-dimensional sampling functions, analogous to

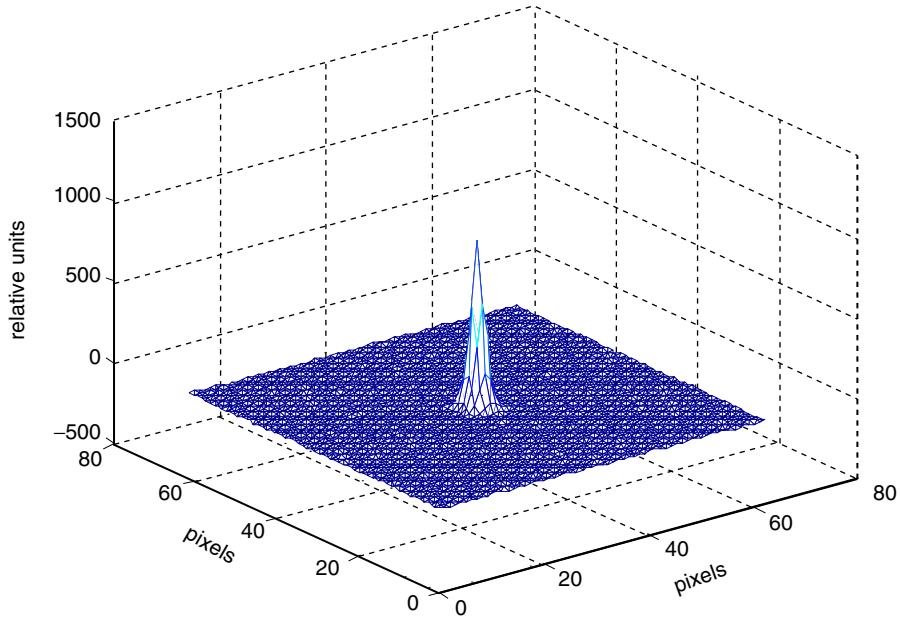

Fig. 3. Two-dimensional sample autocorrelation function over the aperture plane: r_0 = 10 cm.

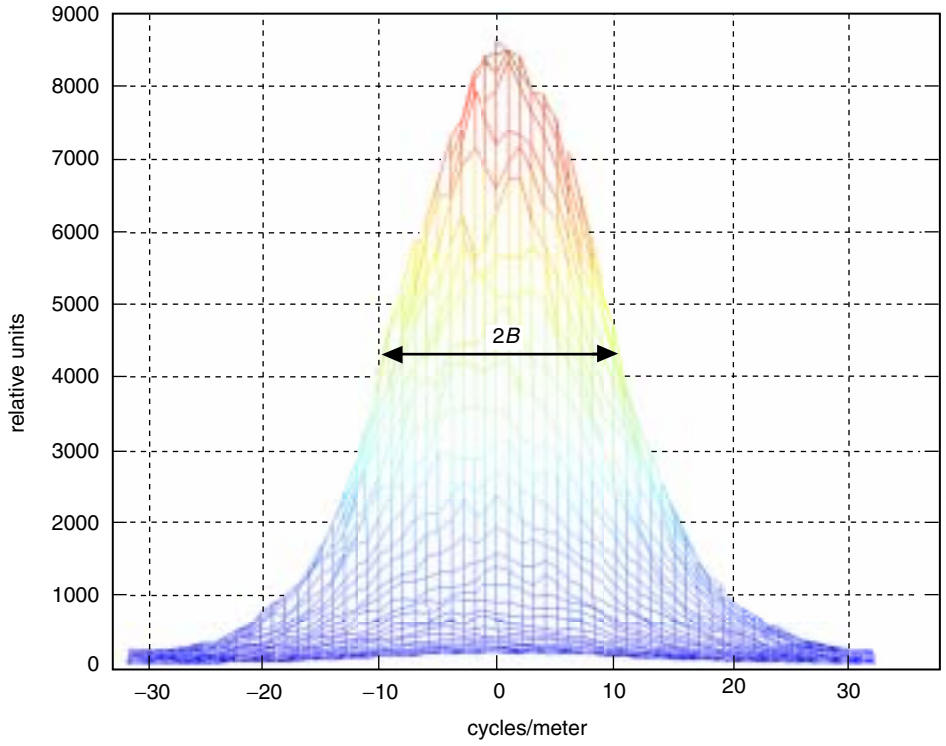

Fig. 4. Power spectrum of the sample field in wave-number space: r_0 = 10 cm.

the time-domain expansion of band-limited time sequences. The canonical sampling functions described in [5] for two-dimensional functions are closely related to the "sinc" function familiar from one-dimensional sampling theory, but functionally depend on the first-order Bessel function $J_1(r)$, where $r = \sqrt{x^2 + y^2}$ is the radial variable along any direction in the aperture plane. If the two-dimensional optical field is limited in wave-number space to $B = \omega/2\pi$ radians, where ω represents the angle of arrival measured from the normal to the aperture plane, then the appropriate sampling functions are of the form

$$\varphi(x, y) = C \frac{J_1\left(2\pi B\sqrt{x^2 + y^2}\right)}{2\pi B\sqrt{x^2 + y^2}} \tag{1}$$

where the normalization C is chosen to ensure that $\iint dxdy\varphi^2(x, y) = 1$.

We observe from Fig. 4 that the effective two-sided bandwidth, $2B$, of the field is about 20 cycles per meter in wave-number space at the 3-decibel point, implying that the bandwidth is approximately given by $B = 10$ cycles per meter; this implies a sample-function spacing of 0.1 meter, or 10 centimeters, consistent with the assumed coherence length of the field.

The two-dimensional expansion functions defined in Eq. (1) can be placed on a regular grid of points corresponding to the first zero-crossing distance of the Bessel function, forming cells of equilateral triangles as shown in Fig. 5. The first three functions so placed are orthogonal, but subsequent functions at various distances from a given grid point are not exactly orthogonal; however, no two functions have greater than a few percent overlap, as shown in [6]. In principle, the set of sampling functions needed to represent any realization of a wave-number-limited optical field over the aperture can be orthogonalized using the Gram–Schmidt procedure [5], resulting in a complete orthonormal set. This complete set of sampling functions then serves as the basis for expanding arbitrary received optical fields over the aperture, with the interpretation that the coefficients are complex samples of the field at the appropriate points in the sampling lattice.

The sampling expansion illustrated in Fig. 5 enables the representation of the instantaneous, or frozen, received optical field, $f(x, y)$, in terms of complex samples $\alpha_{i,j}$ over a grid of points defined by the vertices of equilateral triangles, whose separation is determined by the turbulence-induced atmospheric coherence length over the aperture plane:

$$f(x, y) = \sum_{(i,j)\in A_{rec}} \alpha_{i,j}\varphi_{i,j}(x, y) = \sum_{(i,j)\in A_1} \alpha_{i,j}\varphi_{i,j}(x, y) + \cdots + \sum_{(i,j)\in A_K} \alpha_{i,j}\varphi_{i,j}(x, y) \tag{2}$$

Here,

$$\alpha_{ij} = \iint_{A_{rec}} f(x, y)\varphi_{ij}(x, y)dxdy \tag{3}$$

and the sampling functions are given by

$$\varphi_{ij}(x, y) = C \frac{J_1\left(2\pi B\sqrt{(x - x_i)^2 + (y - y_j)^2}\right)}{2\pi B\sqrt{(x - x_i)^2 + (y - y_j)^2}}$$

where x_i and y_j are the sampling point coordinates. These sampling functions are approximately orthonormal, i.e.,

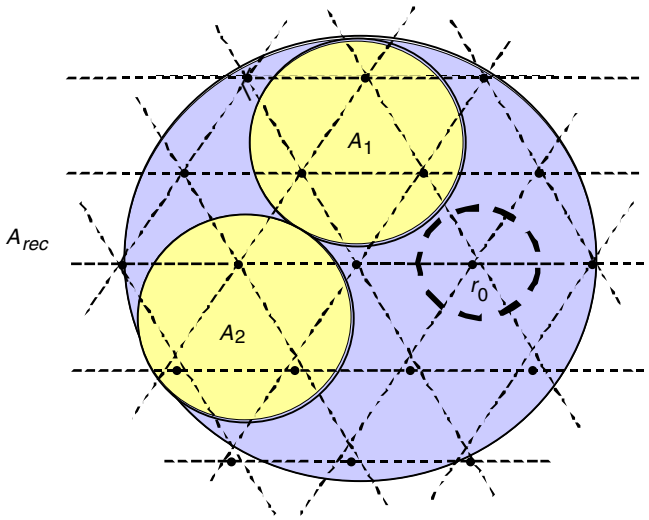

Fig. 5. Sampling grid over the receiver aperture defining placement of sampling functions and illustrating the interpretation of the field as samples over the entire aperture and over two subapertures.

$$\iint\limits_{A_{rec}} \varphi_{ij}^2(x,y)dxdy \approx 1$$

and

$$\iint\limits_{A_{rec}} \varphi_{ij}(x,y)\varphi_{kl}(x,y)dxdy \approx 0, \quad i \neq k, j \neq l$$

As shown in Fig. 5, the coefficients α_{ij} represent samples of the field over the (i,j)th grid point. Due to the circular symmetry and unimodal nature of the two-dimensional sampling functions defined in Eq. (1), these samples may be interpreted as effective coherent areas of radius r_0 centered over each grid point shown by the dashed circle in Fig. 5. Note that we have not taken into account boundary conditions at the edge of the aperture; nor have we formally applied the Gram–Schmidt procedure to fully orthogonalize the basis functions. Therefore, this representation is somewhat approximate but is sufficiently accurate to motivate the development of optical array receiver theory starting with a single large aperture.

If we take the magnitude squared of the complex received field and integrate it spatially over the entire aperture, we obtain the power of the signal field through the aperture. Applying this operation to both sides of Eq. (2) yields

$$\iint\limits_{A_{rec}} dxdy\big|f(x,y)\big|^2 = \iint\limits_{A_{red}} dxdy\left|\sum_{(i,j)\in A_{rec}} \alpha_{ij}\varphi_{ij}(x,y)\right|^2 \cong \sum_{(i,j)\in A_{rec}} \big|\alpha_{ij}\big|^2 \tag{4}$$

where the last expression follows from the approximate orthonormality of the sampling functions. Since the left side of Eq. (4) represents the total power of the signal, so does the right-hand side, with the interpretation that the signal power over the receiver aperture can be built up from the sum of the

individual sample powers. Equivalently, the total power through the aperture can be viewed as the sum of powers collected by small effective apertures centered over each grid point. Note that if the field coherence length is equal to or greater than the diameter of the receiver aperture, then a single sampling function suffices to represent the field: in this case, there is only one coefficient in the expansion, and the total signal power through the aperture equals the squared magnitude of the sample representing the entire received optical field.

Summarizing the key features of the array model, we conclude the following:

(1) The amount of background power collected by any diffraction-limited receiver aperture is a constant independent of the aperture dimensions, because the diffraction-limited field of view (steradians) is inversely related to the receiver area.

(2) The amount of coherent signal power collected by a diffraction-limited receiver is directly proportional to the collecting area. For the case of free-space (not turbulent) reception, the signal is in the form of a plane wave that represents a uniform power density in units of power per unit area; for the turbulent case, the plane wave is broken up into small coherence areas over the collecting aperture, but the total average signal power collected by the receiver remains the same.

Based on the above model, the following general conclusion follows:

(3) A necessary condition to ensure that total signal and noise powers collected by an array of subapertures is of the same total area as a single large receiver is that each subaperture contain at least one sampling coefficient.

This conclusion follows from the interpretation of the sample coefficients as small coherence areas surrounding the center of each sampling function, with effectively constant (complex) value throughout. This model effectively replaces the continuous field model with a discrete representation, where now the total power through the aperture is the sum of the squares of the coefficients. In effect, we have replaced integration over a continuous area with a sum of discrete terms, where each coefficient represents power flowing through a small area over the aperture; these equivalent areas are disjoint and cover the entire aperture. Subapertures containing more than one sample of the field can be constructed in a similar manner, as shown in Fig. 5, conserving energy since the total power flowing through a given subaperture can be estimated by counting the number of discrete signal-field samples it contains.

Whereas the signal energy per sample collected by a coherence area can be estimated directly from the coefficients, the background power cannot, since it is not coherent over the same area as the turbulence-degraded signal field; the background energy is more easily estimated from the conventional plane-wave decomposition illustrated in Fig. 2. However, since the total background power collected by any diffraction-limited receiver is the same, it follows that each coherence area represented by an aperture-plane sample collects P_b^* microwatts of background power. Therefore, according to this model, the total signal power collected by a subaperture containing K samples is proportional to $\sum_{k=1}^{K} |\alpha_k|^2$, whereas the total background power is proportional to $K\,P_b^*$. This conclusion is correct for any subaperture containing at least one sample, from the smallest area with diameter equal to a coherence length to the largest single-aperture receiver containing a great many coherence areas. We conclude that, as long as each subaperture contains at least one signal sample, the total amount of signal and background energy can be built up from the primitive coherence-area samples, and therefore a single large aperture can be constructed as the sum of non-overlapping subapertures with an equivalent collecting area. This model holds over any region on the ground where the turbulence parameters are constant, typically on the order of hundreds of meters or more, and hence over areas much greater than any single-aperture receiver under consideration. Therefore, the centers of the subapertures can be separated by relatively large distances, creating an array from the single large aperture receiver, without affecting the collected signal power and the collected

background power. Arrays of receivers therefore are equivalent to a single-aperture receiver of the same collecting area in the sense that both collect the same total signal and background power, as asserted in conclusion (3), stated above.

However, these conclusions do not extend to the case where the diameters of the array elements become smaller than the atmospheric coherence length. The reason is that, as the coherence area is subdivided into smaller apertures while holding the total area constant, creating in effect subsample apertures, the signal power flowing through each subsample aperture remains proportional to the subsample area, thus conserving signal power, but the background noise power flowing into each subsample aperture is a constant independent of collecting area. This means that each subsample aperture collects less signal power while collecting the same background power; therefore, receiver performance suffers. Alternatively, the total signal power collected by a full-sample aperture and the equivalent array of subsample apertures remains constant as the number of array elements increases, but the total noise power increases proportionally with the number of array elements. A direct consequence of this behavior is the observation that in the absence of turbulence, so that the field coherence length is equal to or greater than the collecting area, subdividing the single aperture into subapertures results in degraded performance when background noise is present. This, of course, is merely a restatement of the fact that coherence areas cannot be subdivided without collecting more noise power than signal power and so incurring a performance loss. We may conclude, therefore, that single-aperture receivers of any diameter can be subdivided into arrays of smaller apertures only if the number of array elements remains smaller than the number of signal samples needed to represent the signal field over the receiver aperture. The above concepts can be restated in terms of the largest single receiver aperture diameter, D, and atmospheric coherence length, r_0:

(4) The performance of an array of small telescopes is equivalent to that of a single-aperture receiver of the same collecting area and diameter, D, provided the number of array elements, $N = KL$ (K detector elements per telescope, L telescopes), obeys the condition $N \leq (D/r_0)^2 \equiv N^*$.

Since the only cause of performance degradation is background radiation, it follows that in the absence of background radiation the total number of array elements, N, is not constrained to be less than N^*. Therefore, in situations where the background radiation is not significant—such as might be the case at night with appropriate narrowband optical filtering—any number of elements could be used to construct an array without suffering performance degradation. However, as a practical matter, the constraint on the number of array elements is not a serious impediment to array design, as the following example illustrates.

Example. It is generally accepted that even under the best possible seeing conditions on the ground, the Fried parameter typically does not exceed 20 centimeters at an operating wavelength of 1 micrometer during the day. If a 10-meter aperture is needed to communicate from deep space, then the maximum number of elements permissible for an array receiver is $N \leq (D/r_0)^2 = (10/0.2)^2 = 2500$. This number is far greater than what is needed to synthesize a 10-meter aperture with reasonably sized telescopes; in fact, with 1-meter apertures, only 100 telescopes would be needed.

We may conclude from this example that, since turbulence is always present during ground reception, an array of telescopes can be constructed with a reasonable number of elements to synthesize a single large-aperture receiver for communications applications.

IV. Array Receiver Performance

In the following analyses, we shall assume that the optical bandwidth of the receiver is great compared to its electrical bandwidth, so that a multimode assumption can be applied to both the signal and background fields. It has been shown that multimode Gaussian fields with suitably small average modal noise count generate approximately Poisson-distributed random-point processes at the output of an ideal

photon-counting detector [2]. This model is reasonable for communications systems operating even at gigabit-per-second rates, and justifies the use of the relatively simple Poisson model which, in turn, often leads to mathematically tractable solutions.

A. Array Detector Model

Consider an array of detectors consisting of $K \times L$ detector elements, representing K detector elements per telescope (FPA) and L telescopes. Assuming a frozen-atmosphere model, the sample-function density of the array of count observables from a particular focal-plane detector element of a given telescope can be written as $p[N_{mn}(t)|\lambda_{mn}(t); 0 \le t < T]$, where $\lambda_{mn}(t)$ and $N_{mn}(t)$ represent the Poisson count intensity and number of counts, respectively, over the mnth detector element, and where m indexes a detector element in the focal plane of the nth telescope [2]. This represents the output of a particular element of the array. Note that if the spatial intensity distribution is known, and the location and size of each detector element are also known, then conditioning on the spatial intensity distribution is equivalent to conditioning on the array of intensity components, each of which is still a function of time. Assuming that each detector element observes the sum of a signal field plus multimode Gaussian noise field, the array outputs can be modeled as conditionally independent Poisson processes, conditioned on the average signal intensity over each detector element. The joint conditional sample-function density over the entire array can be expressed in terms of the KL dimensional vector $\mathbf{N}(t)$ as

$$p\big[\mathbf{N}(t)|\lambda(t); 0 \le t \le T\big] = \prod_{m=1}^{K} \prod_{n=1}^{L} p\big[N_{mn}(t)|\lambda_{mn}(t); 0 \le t < T\big] \tag{5}$$

where $\mathbf{N}(t) \equiv \big(N_{11}(t), N_{12}(t), \cdots, N_{KL}(t)\big)$. This detection model can be used as a starting point for problems involving hypothesis testing and parameter estimation, where the desired information is contained in the intensity distribution but only the array of count accumulator functions can be observed.

B. Hypothesis Testing with Poisson Processes

Consider M-ary pulse-position modulation (PPM) in which one of M intensity functions is received, and the receiver attempts to determine the correct symbol based on observations of the array of count accumulator functions over each of M time slots. It is assumed that the symbol boundaries are known and that the arrival time of each detected photon and the total number of detected photons can be stored for a limited duration of time necessary for processing.

With M-ary PPM modulation, a signal pulse of duration τ seconds is transmitted in one of M consecutive time slots, resulting in a PPM symbol of duration $T = \tau M$ seconds. As shown in [2], the log-likelihood function can be expressed as

$$\begin{aligned} \Lambda_i(T) &= \sum_{m=1}^{K} \sum_{n=1}^{L} \left\{ \sum_{w_{j,mn} \in ((i-1)\tau, i\tau]} \ln\left(1 + \frac{\lambda_{s,mn}(w_{j,mn})}{\lambda_b}\right) \right\} \\ &= \sum_{m=1}^{K} \sum_{n=1}^{L} \ln\left(1 + \frac{\lambda_{s,mn}}{\lambda_b}\right) N_{mn}^{(i)} \end{aligned} \tag{6}$$

where $w_{j,mn}$ is the occurrence time of the jth photon over the mnth detector element within the ith time slot, $N_{mn}^{(i)}$ is defined as the total number of photons occurring over the mth detector element in the focal plane of the nth telescope during the ith time slot, $\lambda_{s,mn}$ is the count intensity due to signal over the mnth detector element, and λ_b is the count intensity due to background noise. Note that with

constant signal intensities the actual arrival times of photons within each slot do not contribute to the decision, hence only the total number of detected photons, $N_{mn}^{(i)}$, matters. Given that we know the intensity over each detector element, the ith log-likelihood function consists of the sum of a logarithmic function of the ratio of signal and background intensities from all detector elements over the ith pulse interval, multiplied by the total number of detected photons; the optimum detection strategy is to select the symbol corresponding to the greatest log-likelihood function.

C. Performance of the Optimum Detector-Array Receiver

The probability of a correct decision is the probability that the log-likelihood function associated with the transmitted symbol exceeds all other log-likelihood functions. Thus, when the qth symbol is sent, then a correct decision is made if $\Lambda_q(T) > \Lambda_i(T)$ for all $i \neq q$. Denoting the logarithmic functions, or weights, in Eq. (6) by $u_{mn}^{(i)}$, the log-likelihood function can be rewritten as

$$\Lambda_i(T) = \sum_{m=1}^{K} \sum_{n=1}^{L} u_{mn}^{(i)} N_{mn} \tag{7}$$

In this form, we can see that the log-likelihood function is composed of sums of a random number of weights from each detector element; for example, the mth detector element in the nth telescope contributes an integer number of its own weight to the sum. Note that detectors containing much more background than signal intensity do not contribute significantly to the error probability, since the outputs of these detector elements are multiplied by weights that are close to zero. This observation suggests the following suboptimum decoder concept with greatly simplified structure: list the detector elements from all telescopes simultaneously, starting with the one containing the most signal energy, followed by every other detector ordered according to decreasing signal intensities. In effect, the logarithmic weights are partitioned into two classes: large weights are assigned the value one, while small weights are assigned the value zero. It was shown previously that this simple partitioning achieves near-optimum performance in low- to moderate-background environments, but with greatly reduced decoder complexity.

The processing to determine which detector elements to use from the array to achieve best performance can be explained as follows: compute the probability of error for the first detector element plus background, then form the sum of signal energies from the first two detector elements (plus background for two detector elements), and so on, until the minimum error probability is reached. The set of detector elements over all telescopes that minimizes the probability of error for the entire array is selected, as this set achieves best performance. However, this straightforward process of performing the optimization is not practical for an array of telescopes, since the output of each detector element must be sent to a central processing assembly, where the computations are performed; while this is conceptually straightforward, the complexity required to achieve this processing with a large number of wideband channels quickly becomes prohibitive.

For the adaptively synthesized array detector, the probability of correct decision given hypothesis q, or H_q, can be obtained by assuming constant signal and background intensities over each time slot, yielding the conditional Poisson densities

$$p_q(k|H_q) = \frac{(\lambda_s\tau + \lambda_b\tau)^k}{k!} e^{-(\lambda_s\tau+\lambda_b\tau)} \tag{8a}$$

and

$$p_i(k|H_q) = \frac{(\lambda_b\tau)^k}{k!} e^{-\lambda_b\tau} \tag{8b}$$

Here we interpret $\lambda_s\tau$ as the total average signal count per PPM slot over the selected set of detector elements when a signal is present, and $\lambda_b\tau$ as the total average background count over the same set of detector elements, per PPM slot. As shown in [2], the probability of correct symbol decision is given by

$$P_M(C) =$$

$$\left\{ \sum_{r=0}^{M-1} \left(\frac{1}{r+1} \right) \binom{M-1}{r} \sum_{k=1}^{\infty} \frac{(\lambda_s\tau + \lambda_b\tau)^k}{k!} e^{-(\lambda_s\tau+\lambda_b\tau)} \left[\frac{(\lambda_b\tau)^k}{k!} e^{-\lambda_b\tau} \right]^r \left[\sum_{j=0}^{k-1} \frac{(\lambda_b\tau)^j}{j!} e^{-\lambda_b\tau} \right]^{M-1-r} \right\}$$

$$+ M^{-1} e^{-(\lambda_s + M\lambda_b)\tau} \tag{9}$$

and the probability of symbol error follows as $P_M(E) = 1 - P_M(C)$.

Performance of the array receiver was evaluated via simulated phase disturbances over each telescope of the array, using Kolmogorov phase screens as described in [7]. A sample field was generated using the distorted phase distribution, resulting in a matrix of complex signal amplitudes over each aperture. For these simulations, an atmospheric correlation length of $r_0 = 10$ centimeters was assumed. The field intensity generated in the detector plane of each telescope was integrated over the elements of a 128×128 pixel detector array, which is assumed to encompass the extent of the signal distribution in the focal plane of each telescope.

The performance of an entire sequence of arrays, starting with one large element representing the single-element receiver implementation and subdividing it into 4, 16, and 64 smaller elements of constant total collecting area, was evaluated in the following manner. Error probability was computed for both ideal turbulence-free conditions and for turbulence characterized by Fried parameter (or coherence length) of $r_0 = 10$ centimeters and an outer scale of turbulence corresponding to 64 meters. In a typical computation, the $128 \times 128 = 16,384$ pixel energies representing the output of a single 4-meter aperture were sorted in decreasing order of average signal energy, and M-ary PPM symbol-error probabilities were calculated for increasing numbers of detectors, starting with the first detector. Let K_s denote the average number of signal photons per PPM slot collected by the entire array aperture when a signal is present, and let k_b denote the average number of background photons per PPM slot collected by a diffraction-limited detector element (generally made up from several contiguous pixels). We also define the total average number of background photons collected by the entire array aperture as $K_b = (D/r_0)^2 k_b$, where D is the diameter of the large single-aperture receiver. However, we should keep in mind that the adaptively synthesized focal-plane detector array typically rejects most of the background radiation, collecting background photons selectively from those detector elements that contain significant signal energy. Figure 6 shows the symbol-error probability for 16-dimensional PPM ($M = 16$) as a function of the number of detector elements used, for the case $K_s = 10$ photons per slot and $k_b = 0.01$ photon per slot per diffraction-limited FOV or, equivalently, $K_b = 4$. It can be seen that for this case the smallest error probability of $10^{-2.7} \approx 0.002$ is achieved by assigning unity weight to the first 50 pixels containing the greatest signal intensities and zero to all the rest.

The same approach was used to determine array receiver performance in the presence turbulence, as shown in Fig. 7. However, in this case the minimum-error probability is obtained with 1200 pixels sorted according to signal energy, instead of 50 as for the diffraction-limited case. In the presence of noise, this means that performance suffers, because 1200 pixels collect approximately 24 times as much background noise as the 50 sorted pixels that attained the minimum-error probability in the absence of turbulence.

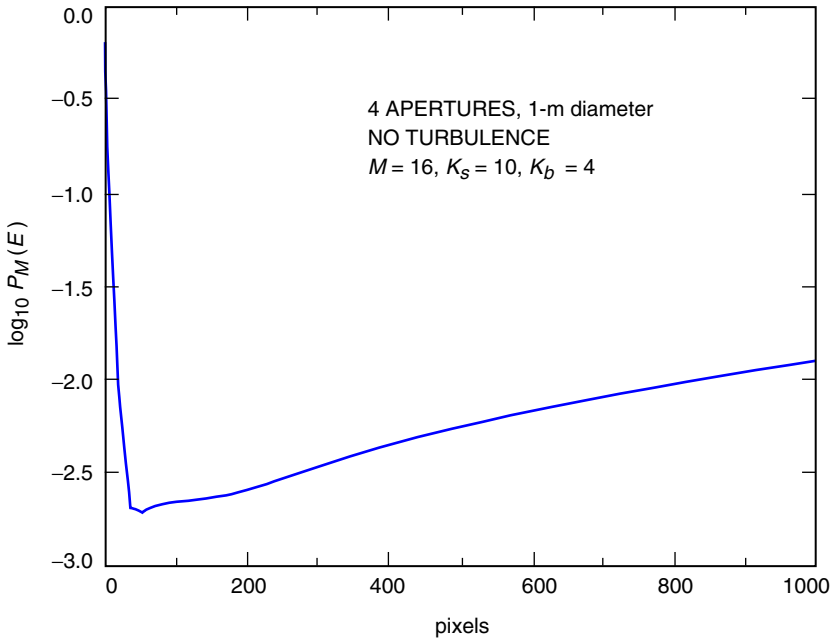

Fig. 6. Probability of error as a function of the number of sorted pixels: no turbulence.

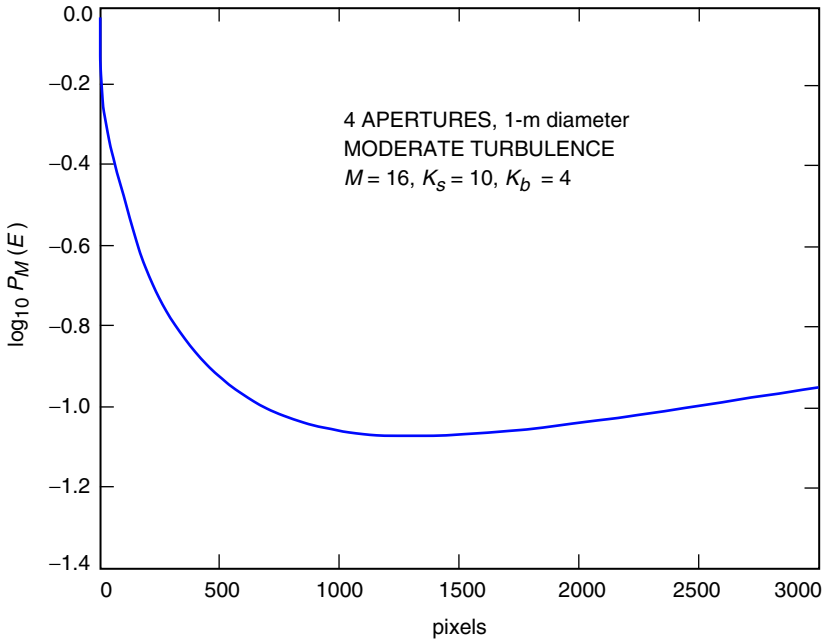

Fig. 7. Probability of error as a function of the number of sorted pixels: moderate turbulence, r_0 = 10 cm.

The performance of the optical arrays was evaluated using the procedure described above to determine the error probability of the adaptive "1-0" receiver. Arrays of various sizes, consisting of increasing numbers of telescopes with proportionally smaller apertures to keep the total collecting area constant, were evaluated. Independent samples of Kolmogorov phase screens were generated for each telescope, and the signal intensity distributions in the focal plane were determined for each sample function, using two-dimensional Fourier transforms. The focal plane of each telescope was assumed to contain a focal-plane array, of dimensions consistent with the telescope diameter and the expected level of turbulence.

In a typical simulation, a large telescope is analyzed first, by determining its performance according to the sorting procedure described above. The probability of error is calculated for increasing amounts of signal energy passing through the aperture, and distributed in the focal plane according to the two-dimensional Fourier transform of the aperture-field distribution generated using the Kolmogorov phase-screen program. Next, the diameter of each telescope was divided by two, generating four smaller telescopes with the same total area as the previous array, and the performance of the new larger array was computed as before. The process of dividing telescope diameters by a factor of two in order to generate the next larger array was continued four times, generating arrays of 4, 16, and 64 elements from a single large telescope. Different realizations of the signal intensity distribution were generated for each element of the new array; thus, a single telescope used a single phase-screen realization over the aperture plane, whereas an array of $N \times N$ telescopes of the same area as the single telescope used a total of N^2 different phase-screen realizations. The intensity distributions were then scaled such that the total signal energy entering the single large-aperture receiver and the array were equal.

An example of the phase distributions generated for analyzing array performance is shown in Figs. 8(a) and 8(b). The variation of optical phase over each telescope, when operating in turbulence with a Fried parameter of $r_0 = 0.1$ meter (or 10 centimeters) and an outer scale of turbulence of 64 meters, is shown in

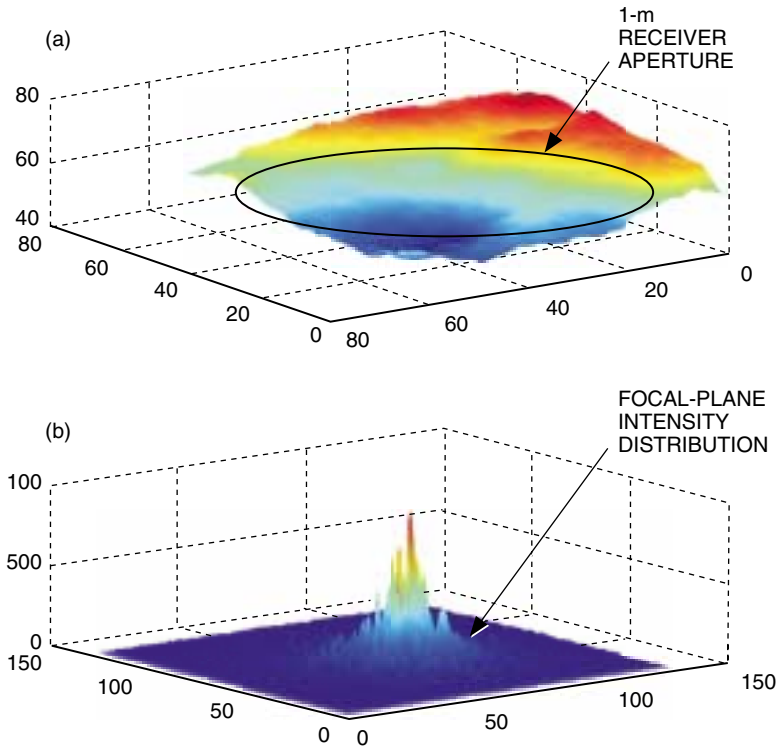

Fig. 8. A single 1-m-diameter telescope, 10-cm atmospheric-coherence length: (a) aperture-plane phase distribution and (b) corresponding focal-plane intensity distribution .

Fig. 8(a); the corresponding focal-plane signal distribution is shown in Fig. 8(b). Note that, because the 1-meter telescope aperture is large compared to the 10-centimeter Fried parameter, there are a great many spatial modes excited by the signal field, and therefore the PSF is significantly distorted with numerous intensity peaks. This implies that a correspondingly large number of detector elements must be used to collect the signal, inadvertently collecting background radiation as well.

Aperture-plane and focal-plane distributions for two out of the four half-diameter telescopes comprising the first-level array are shown in Fig. 9. Note that with the smaller apertures and moderate turbulence as before, the PSF remains peaked and highly concentrated in the focal plane, suggesting that most of the signal energy is now localized in each telescope. However, due to the larger number of telescopes in the array, the same number of modes is observed as with the single large-aperture telescope, and therefore the same amount of background radiation is collected.

The process of dividing each telescope diameter to create larger arrays can be continued indefinitely in principle, yielding second-, third-, and higher-generation arrays, each containing four times as many elements as the previous configuration. However, continuing this process makes sense only as long as the telescope diameters exceed the Fried parameter; after that point, further reductions in telescope size lead to degraded performance for the reason described in Section III. As the total number of telescopes in the array begins to exceed the total number of signal modes, it is no longer possible to distribute the signal power over more telescopes without incurring additional penalties due to the excess background radiation collected by the array. This behavior is illustrated by the performance curves in Fig. 10, which show the performance of a single 2-meter aperture, together with arrays of 4, 16, and 64 elements of diameter 1 m, 0.5 m, and 0.25 m, respectively, under two scenarios: first, the performance of the array is determined under negligible-turbulence conditions (as might be the case for a space-borne array); and second, the performance with turbulence of 10-centimeter coherence length was determined for 16-PPM signals. Background radiation of 0.01 photon per diffraction-limited FOV per slot was assumed for these calculations.

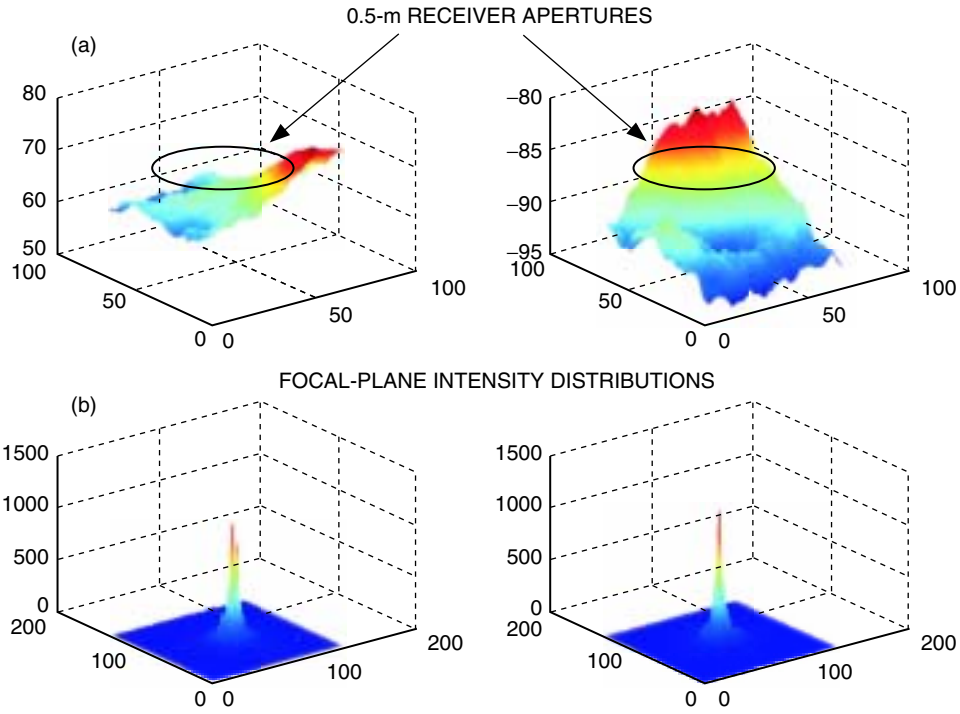

Fig. 9. Two telescopes of a larger array, 0.5-m diameter and 10-cm atmospheric-coherence length: (a) aperture-plane phase distributions and (b) corresponding focal-plane intensity distributions.

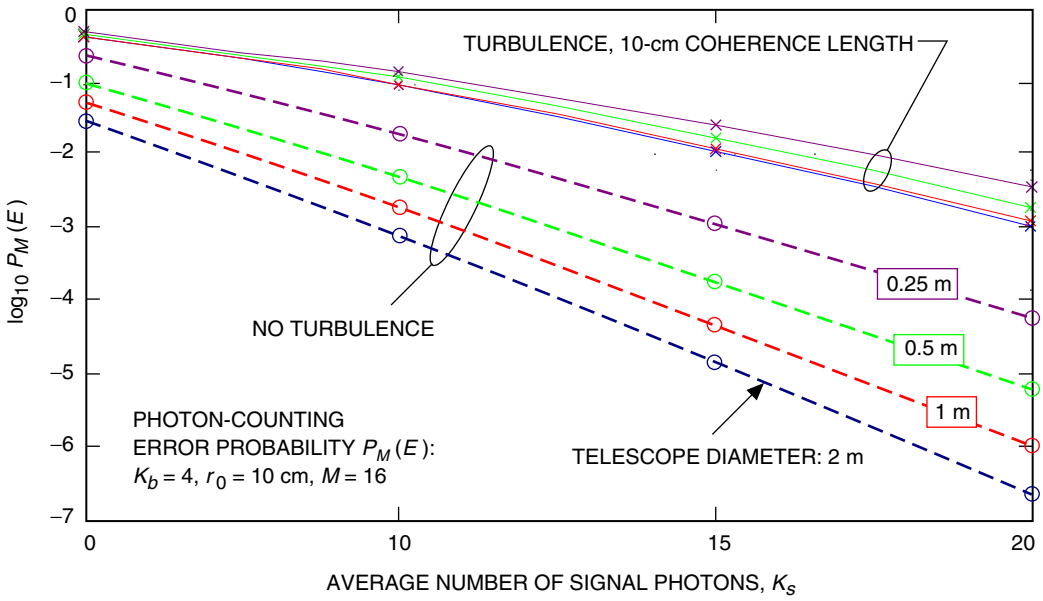

Fig. 10. Performance of a single 2-m telescope and an equivalent-aperture array receiver, with and without turbulence.

Figure 10 shows that with little or no turbulence, such that $r_o > D$, the single large receiver performs best. However, with significant turbulence, $r_o \ll D$, the array performance is comparable to that of a single large receiver.

Note that in the absence of turbulence a single large-aperture receiver performs best because the signal is in the form of an undistorted plane wave, and therefore a single detector element with diffraction-limited FOV suffices to collect essentially all of the signal energy. At the same time, background radiation entering the receiver from all directions within the FOV can be maximally suppressed, only the minimal amount within the small diffraction-limited cone of angles contributing to background interference within the receiver. Since diffraction-limited FOV and collecting area are inversely related, the amount of background radiation in a diffraction-limited FOV is independent of receiver aperture; this means that N diffraction-limited receivers collect N times as much background energy as a single receiver, regardless of telescope diameter. Therefore, arrays of diffraction-limited receivers collect background energy proportional to the number of elements, not proportional to the total collecting area. The performance of diffraction-limited arrays observing a signal in the absence of turbulence but with moderate background radiation in the diffraction-limited FOV of each telescope is illustrated in Fig. 10; note that performance degrades significantly as the number of array elements increases from a single 2-meter-diameter telescope to 4 telescopes of 1-meter aperture, then to 16, and finally to 64 telescopes of 0.25-meter diameter.

However, turbulence is ever present; even in good seeing (corresponding to a Fried parameter of 10 centimeters or more), the performance of the first-generation array (of 4 telescopes) is virtually indistinguishable from the performance of the single aperture, as the performance curves corresponding to turbulent conditions indicate. This occurs because in the presence of turbulence the single telescope must increase its FOV well beyond the diffraction limit to collect sufficient signal energy to minimize the probability of symbol error, and in the process collects more background energy as well. In effect, the single-aperture receiver must observe more than one (typically, a great many) spatial modes, each mode approximated by a diffraction-limited FOV collecting both signal and background energy from slightly different directions. The array of small telescopes observes the same total number of spatial modes, and hence collects the same amount of background energy by the above argument. Since the total collecting

area of the array is the same as that of the single receiver, it also collects the same amount of signal energy; therefore, the performance of the array is essentially the same as that of the single-aperture receiver. Small variations in the array performance curves with turbulence are due to slight variations of the random phase distributions generated by the Kolmogorov phase-screen program.

D. Extrapolating to Determine the Performance of Large Arrays

In order to determine if there is a "best" array telescope diameter, array performance was evaluated for a given value of total signal energy, background intensity, and turbulence parameter for a large number of arrays. As originally developed, computations for array performance can be carried out in a reasonable amount of time (approximately 1 hour per run) for arrays of no more than 64 elements. This allows analysis of arrays consisting of up to 4 different telescope sizes (for example, 2 meter, 1 meter, 0.5 meter, and 0.25 meter). It was found that increasing the array size beyond 64 elements, with each array containing its own focal-plane array of detectors, began to incur unacceptably great computational burdens. Therefore, an approach was developed to evaluate the performance of a large array by modifying the input noise parameters of smaller arrays, and then "connecting" the results in order to estimate performance over a much larger range of array diameters.

This technique was first applied to arrays of telescopes with diameters ranging from a single telescope of 4-meter diameter to an array of 0.125-meter telescopes, creating arrays of 1, 4, 16, 64, 128, and 512 elements. These arrays were split into two sets: the first set consisted of 4-meter, 2-meter, 1-meter, and 0.5-meter telescopes, while the second set consisted of 1-meter, 0.5-meter, 0.25-meter, and 0.125-meter telescopes. The noise parameters of the second set were increased by a factor of four to account for the total noise power collected by an array with four times the number of elements, and the performances of the two sets computed using the initial program. Three different test cases were run with an average of 20 signal photons and moderate background noise of 0.01 photon per PPM slot per diffraction-limited field of view. This implies that the average number of background photons collected by the entire array aperture is $K_b = (4/0.1)^2 \times 0.01 = 16$, which represents an extremely high background environment. The results of the individual runs shown in Fig. 11 indicate that the two sets could indeed be connected, resulting in greatly simplified computations. Small differences in the performance of the two sets at aperture diameters of 0.5 meter and 1 meter are attributed to variations in the sample functions of the focal-plane signal energy distributions generated by the phase-screen programs. Note that as the

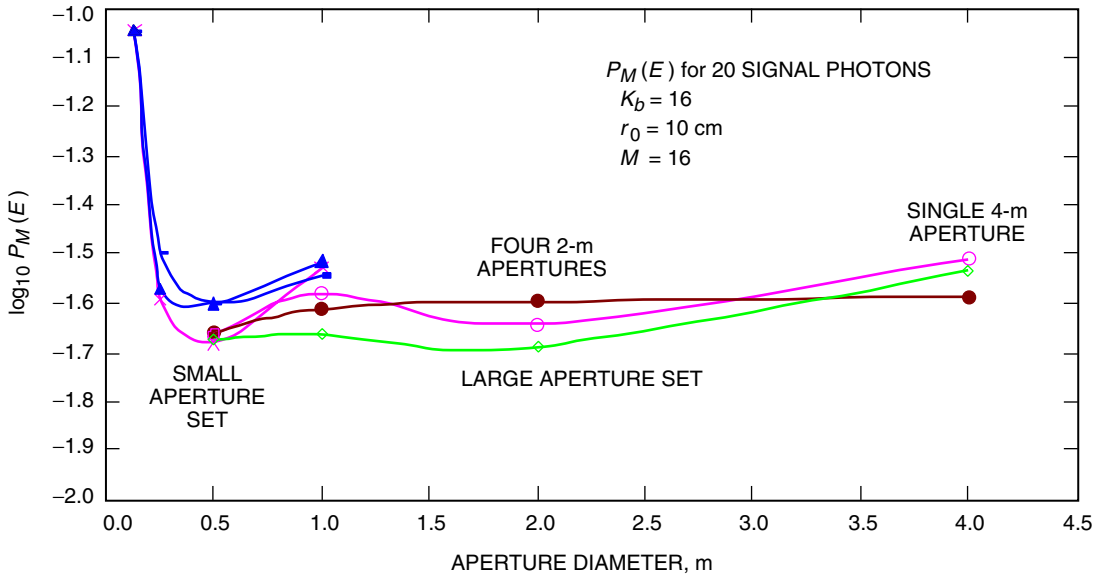

Fig. 11. Results of tests for evaluating the connectivity of small arrays.

telescope diameters approach the Fried parameter performance deteriorates in all cases. The modal analysis presented in Section III predicted this performance degradation for apertures smaller than the coherence length; however, it is actually observed for somewhat larger collecting areas in Fig. 11. This behavior is attributed to the fact that the modal analysis was only approximate, and did not take into account edge effects that start to become significant under these conditions.

Taking the average of the performance curves of Fig. 11 at each telescope diameter yields the averaged performance curve of Fig. 12, which shows a smooth continuous curve through the entire range of diameters from 4 meters to 0.125 meter, supporting the validity of the approach. Figure 12 also shows the hypothetical performance of the diffraction-limited receiver, corresponding to turbulence-free conditions, but observing the same background radiation (a condition that can only be approached in free space for large apertures). Since without turbulence a single field sample suffices to represent the aperture-plane field, and hence only one diffraction-limited unit of background power is collected, the performance of the arrays is always better in the absence of turbulence.

Finally, these results were extended to cover a range of telescope diameters from 8 meters to 0.125 meter, again using the connected-set approach and averaging a large number of runs to obtain the final results. The results for arrays with the 8-meter collecting area are shown in Fig. 13. These results are similar to the previous 4-meter case shown in Fig. 12, except that performance is uniformly worse for the following reason: with atmospheric coherence length, signal energy, and background intensity held constant for both cases, the total number of signal modes is four times as great for the 8-meter equivalent aperture as for the 4-meter aperture. This means the larger 8-meter array collects four times as much background energy while collecting the same signal energy as the 4-meter array, and hence appears to suffer degraded performance. Similar performance would be achieved by the larger array if the signal energy were increased proportionally to the area.

In the above examples, the total number of focal-plane pixels at each telescope was not limited to any specific value a priori; in fact, every attempt was made to make sure that enough detector elements were used to collect all of the signal energy for each sample function of the phase distribution. This approach is not practical, however, since in a physical realization the number of pixels will be limited due to complexity and implementation considerations. The performance of the array with realistic constraints imposed on

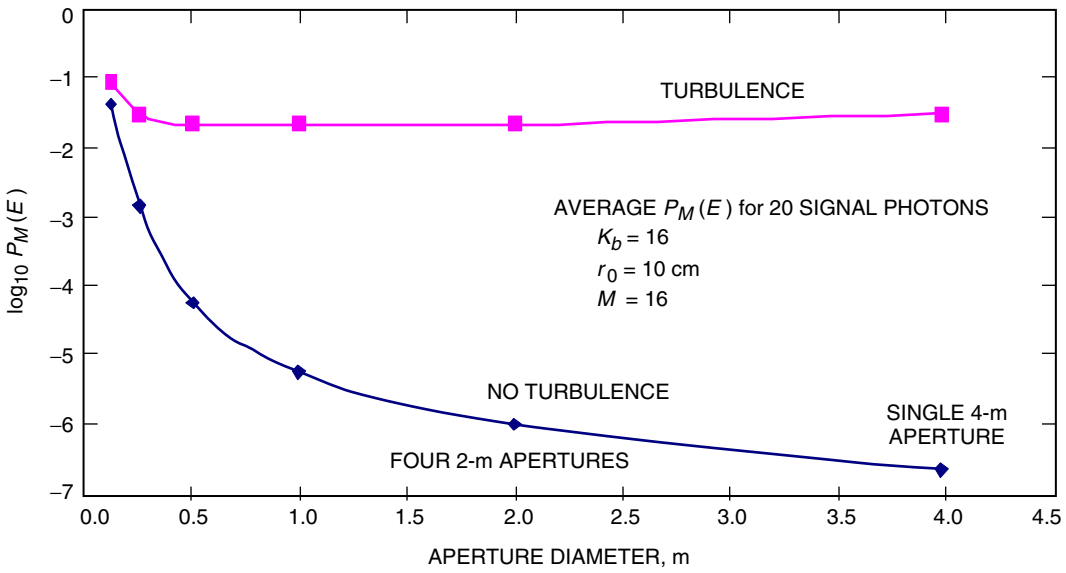

Fig. 12. Averaged performance of 4-m-equivalent arrays, 20 signal photons, 0.01 noise photon per slot.

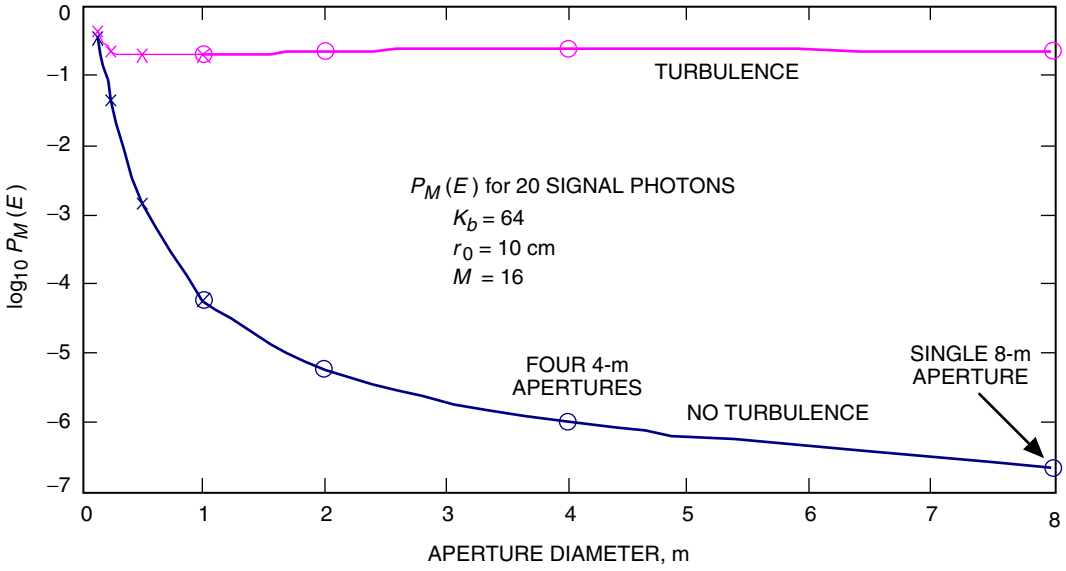

Fig. 13. Averaged performance of 8-m-equivalent arrays, 20 signal photons, 64 noise photons per slot. Note the degraded performance relative to the 4-m array, due to increased background noise while keeping the average signal energy the same.

key array parameters, along with experimental results obtained from the recently acquired 64-cm-diameter New Technology Telescope and the Santa Barbara Instruments Group (SBIG) data-acquisition assembly, will be investigated in a future article.

V. Conclusions

The concept of an optical array receiver suitable for deep-space communications has been defined, and the theoretical foundations of optical array receiver operation and performance has been established. The necessary mathematical models for representing aperture-plane and focal-plane fields have been developed, and detection theory has been applied to determine the performance of an optical array receiver under realistic operating conditions. In particular, the performance of multi-element telescope arrays observing pulse-position modulated optical signals in the presence of atmospheric turbulence and background interference has been investigated, and conditions have been determined under which array performance and single-aperture receiver performance were identical. The performances of various array configurations have been determined and shown to be equivalent to the performance of the large single-aperture receiver, thus demonstrating that the array approach does not incur any losses relative to the single-aperture approach under operating conditions of interest.

Based on the above results, we conclude that the array receiver concept represents a viable alternative to the more conventional approach of using a single large-aperture telescope to collect the optical signal energy, particularly since high-data-rate reception from the depths of space demands ever increasing collecting areas to achieve the desired performance. Large-aperture telescopes are difficult to construct and maintain, require massive support structures and drive assemblies, and pose the risk of jeopardizing the mission in case of failure. In addition, once constructed, the collecting area of a single telescope cannot be easily expanded to meet demands for increased performance. An array of small telescopes, on the other hand, provides a robust, scalable, parallel receiver architecture that can easily be expanded to meet greater demands with relative ease.

References

[1] R. Gagliardi and S. Karp, *Optical Communications,* New York: John Wiley and Sons, 1976.

[2] V. Vilnrotter and M. Srinivasan, "Adaptive Detector Arrays for Optical Communications Receivers," *IEEE Transactions on Communications,* vol. 50, no. 7, pp. 1091–1097, July 2002.

[3] W. Pratt, *Laser Communications Systems,* New York: John Wiley and Sons, 1969.

[4] J. W. Goodman, *Introduction to Fourier Optics,* New York: McGraw-Hill, 1968.

[5] D. Petersen and D. Middleton, "Sampling and Reconstruction of Wave-Number-Limited Functions in N-Dimensional Euclidian Spaces," *Information and Control,* vol. 5, pp. 279–323, 1962.

[6] V. Vilnrotter, *Focal-Plane Processing for Scattered Optical Fields,* Ph.D. Dissertation, University of Southern California, June 1978.

[7] P. Negrete-Regagnon, "Practical Aspects of Image Recovery by Means of the Bispectrum," *Journal of the Optical Society of America,* vol. 13, no. 7, pp. 1557–1576, July 1996.